NPS-57Zi74112

ION
SCHOOL
RNIA 93940

NAVAL POSTGRADUATE SCHOOL

Monterey, California

ELECTROGASDYNAMIC SPECTRAL ANEMOMETER

OSCAR BIBLARZ

1 November 1974

Approved for public release; distribution unlimited

FEDDOCS
D 208.14/2:NPS-57Zi74112

pared for
val Air Systems Command
shington, D.C. 20361

NAVAL POSTGRADUATE SCHOOL
Monterey, California

Rear Admiral I. W. Linder
Superintendent

Jack R. Borsting
Provost

This work is the outgrowth of research sponsored by the Naval Air Systems Command, under AIRTASK A310310C/551A/2 R02401-001. A patent (Navy Case No. 54,466) has been obtained for the device described herein.

Reproduction of all or part of this report is authorized.

This report was prepared by:

REPORT DOCUMENTATION PAGE		READ INSTRUCTIONS BEFORE COMPLETING FORM
1. REPORT NUMBER NPS - 57Zi74112	2. GOVT ACCESSION NO.	3. RECIPIENT'S CATALOG NUMBER
4. TITLE (and Subtitle) ELECTROGASDYNAMIC SPECTRAL ANEMOMETER		5. TYPE OF REPORT & PERIOD COVERED 6. PERFORMING ORG. REPORT NUMBER
7. AUTHOR(s) OSCAR BIBLARZ		8. CONTRACT OR GRANT NUMBER(s)
9. PERFORMING ORGANIZATION NAME AND ADDRESS NAVAL POSTGRADUATE SCHOOL MONTEREY, CALIFORNIA 93940		10. PROGRAM ELEMENT, PROJECT, TASK AREA & WORK UNIT NUMBERS R02401-001, WR 2-6059
11. CONTROLLING OFFICE NAME AND ADDRESS NAVAL AIR SYSTEMS COMMAND WASHINGTON, DC 20361		12. REPORT DATE November 1, 1974 13. NUMBER OF PAGES 40
14. MONITORING AGENCY NAME & ADDRESS (if different from Controlling Office)		15. SECURITY CLASS. (of this report) UNCLASSIFIED 15a. DECLASSIFICATION/DOWNGRADING SCHEDULE

16. DISTRIBUTION STATEMENT (of this Report)

Approved for public release; distribution unlimited.

17. DISTRIBUTION STATEMENT (of the abstract entered in Block 20, if different from Report)

18. SUPPLEMENTARY NOTES

19. KEY WORDS (Continue on reverse side if necessary and identify by block number)

20. ABSTRACT (Continue on reverse side if necessary and identify by block number)

A device which may complement the hot-wire anemometer and the laser velocimeter is the electrogasdynamic (EGD) spectral anemometer. The conception of this instrument and some preliminary measurements represent the body of this report. The EGD anemometer consists of an injector of unipolar charged particles fed into the flow to be probed, an equilibration region, and a collector for the charges. The particles are many times heavier than the molecules in the gas and they interact with the flow through drag forces. If these

DD FORM 1 JAN 73 1473 EDITION OF 1 NOV 65 IS OBSOLETE
(Page 1) S/N 0102-014-6601 |

particles are tightly coupled to the flow, then the collecting probe receives information in electrical form about the fluid velocity. Besides being a direct velocity measurement, the probe can be of streamlined shape and very rugged, and it is insensitive to temperature differences in the flow. The charged particles can be chosen so as to give the desired range of frequency response. The instrument is sensitive to impurities in the flow but in principle the effect may be calibrated out.

An EGD spectral anemometer has been tested using water droplets charged as they condense through a corona discharge. The anemometer consists of a short-circuited EGD generator; this is the first time that such an application has been reported and a Navy patent has been awarded for this device. The feasibility of the anemometer depends on the magnitude of the charged particle slip. The coupling between the flow field and the electric field depends on the frequency range of the velocity fluctuations as well as on the charge, size, and mass of the particles. The work treats the mass as a first order perturbation, in the particle momentum equation. The unsteady flow studied is a region in the wake of a cylinder where charged water droplets are injected into an air flow. From this work the size of the charged particles is calculated and a correspondence is found between the mean particle size injected and the observed frequency response of the anemometer tested. The EGD spectral anemometer data are compared to hot-wire data taken at the same location; some results compare within ± 2 dbs up to a frequency of 630 Hz whereas others are within ± 6 dbs up to 20 KHz. The parameters which varied are the steam pressure and temperature, and the corona characteristics. Predictions of frequency response as a function of charged particle size are given.

TABLE OF CONTENTS

PAGE

DD Form 1473 - ii

Table of Contents - iv

List of Figures - v

Preface - 1

I. Introduction - 2

II. EGD Anemometer - 3

III. Concepts from Unsteady Flow - - - - - - - - - - - - - 5

IV. Experimental Set-up - - - - - - - - - - - - - - - - - 11

V. Results and Discussion - - - - - - - - - - - - - - - - 16

Appendix A - 29

Appendix B - 35

References - 38

Distribution List - 39

LIST OF FIGURES

PAGE

Figure 1 - Maximum Drift Due to Electric Field for Water Droplets in Air at 1-Atm and $20^{\circ}C$ 6

Figure 2 - Optimum Frequency Response as a Function for the Radius 8

Figure 3 - EGD-Generator Schematic 12

Figure 4 - Aerosol Injector 13

Figure 5 - Electrical Schematic of Collector 15

Figure 6 - Composite of Hot-Wire Anemometer Data 17

Figure 7 - Comparison of EGD and Hot-Wire Data 19

Figure 8 - Comparison of EGD and Hot-Wire Data 20

Figure 9 - Comparison of EGD and Hot-Wire Data 21

Figure 10 - Comparison of EGD and Hot-Wire Data 22

Figure 11 - Effect of Density on Current Efficiency 25

Figure 12 - Optimum Voltage and Current 26

Figure 13 - Effect of Temperature on High Frequency Response as a Function of Current Efficiency 28

Figure 14 - One-Dimensional Model 30

Figure 15 - Plot of $(1-\tau^2\omega^2)$ versus Radius for 500 Hz and 16,000 Hz 37

PREFACE

The author would like to acknowledge the participation of the following students during various stages of this work:

LT R. A. Christianson MS(1970)

LT R. J. Laib MS(1971)

The laser holographic measurements were carried out with the guidance and assistance of Professor D. J. Collins of the Aeronautics Department of NPS.

I. INTRODUCTION

Electrofluiddynamic devices operate on the principle that a nonconducting fluid can interact with an electric field when unipolar charges are introduced into the fluid. If this interaction does not disturb the fluid appreciably and if the charged particles are linked intimately with the flow, then the arrival of these particles at a suitable collector brings information about characteristics of the flow. This work deals exclusively with gases and the term electrogasdynamic (EGD) anemometer will be used to denote the device under consideration.

The feasibility of the anemometer hinges on the proper choice of charged particles. These must couple the gas to the electric field through individual collisions if the particles are small enough or through fluid dynamic drag and pressure forces, if they are large enough. Molecular ions are too mobile to be useful[1]; therefore, charged particles of size much larger than the gas molecules must be introduced. The ultimate size of these particles is restricted by their ability to follow the turbulent fluctuations and by the fact that, depending on the method of charging, a large particle may have a sizeable mobility (as will be seen in Section III). In this paper, the effect that particle size and charge have on the coupling between the fluid and the electric field will be discussed.

It may be mentioned in passing that the definition of particle slip in unsteady flow is not only crucial for the anemometer but also for the EGD-power generator. Since turbulence is a means of enhancing the breakdown strength in a gas[2,3] and since generators[1,4] rely on the mixing of fluids both to increase the pressure drop in the channel and to insulate, there must exist regions of unsteadiness in the flow. Hence, a small

slip parameter for steady flow may misrepresent the ability of a charged particle to interact with the flow.

II. EGD - Anemometer

When a charged particle is tightly coupled to the flow, it is essentially a flow "tracer." To pick up such a tracer one simply places a metallic probe which provides the neutralizing current. The injected charges need a certain time to equilibrate with the flow but thereafter they drain no energy from the flow. The particles are neutralized as they arrive with the surrounding gas and are not forced to the probe by an external field hence, in principle, the probe does not distrub the nature of the flow.

Because the collection area is not necessarily the probe area[1] and because of an uncertainty in the size and charge of the particles, it is expedient to measure the spectral characteristics of the flow independently with a hot-wire anemometer and then to compare the results with those of the EGD-anemometer. This permits the optimization of the operating parameters of the EGD-anemometer and allows the inference of charge and size distributions for the charged particles.

The hot-wire anemometer, although a heat transfer measurement, has emerged as perhaps the most useful device for measurements in unsteady flows. Needless to say, advances in fluid mechanics hinge on reliable measurements, and hot-wire data are an accepted standard for these measurements. The EGD device can complement the hot-wire anemometer.

An EGD-anemometer consists of the following: an injector or source for the charged particles, a conversion region where the particles equilibrate with the flow, and a collector for the charges. The collector unit corresponds to the anemometer probe. The EGD-probe is very rugged, allowing the probing of intense turbulent fields. It is simple and

inexpensive, and therefore can be easily manufactured. Since very small charged particles can react to high frequency oscillations, the frequency response of the EGD-probe can be as high as the best hot-wire (at no compromise in mechanical strength). In addition, signals from the EGD-probe are electrical and need little or no further amplification. Effects corresponding to the thermal inertia of hot-wires are not present. There is no need for a linearizer since the EGD measurement is already linear, i.e., a direct measurement. Absent are the complications that free convection currents bring to the hot-wire zero setting. In the case of two-phase flows, the EGD-probe needs no separate calibration and will withstand the impact of charge droplets or solid particles whereas the fragile hot-wire will readily break under these conditions. In the case of two mixing jets, there will invariably be a temperature difference and this, however slight, will affect the hot-wire since it is sensitive to temperature differences. The geometry of the EGD probe is more adaptable than that of the hot-wire to unusual probing situations.

The main disadvantage of the EGD scheme for anemometry is the requirement for a source of particles of optimum size and charge. If the particles are created through a corona discharge then there is a need for a high voltage supply (with the associated safety precautions). Also, the injector/collector unit must have a separation of the order of millimeters and must be traversable all of which pose several design problems. However, all these problems can be overcome and the use of an EGD-generator scheme as a spectral anemometer looks quite feasible.

It should be pointed out that the use of charges in a flow for anemometry is not entirely a new idea. Hinze[5] describes electric discharge anemometers which consist typically of a glow or corona discharge in the flowing medium. More recently, Nygaard[6] has worked on a type of corona-discharge anemometer. A mass flow meter device based on an ion-displacement concept of Professor Durbin[7] is being marketed by Thermo-Systems, Inc.

None of the reported schemes, however, have concentrated on the spectral response of the instrument and, in particular, in matching the charged particles to the desired value of the slip at a given frequency range.

III. Concepts from Unsteady Flow

The ability of a charged particle to couple its surrounding gas to the electric field is described by its slip. The drift velocity with which a charged particle moves in an electric field is given by the product of its mobility (μ) times the electric field (E)

$$v_D = \mu E \tag{1}$$

and the slip (S) for steady flow is defined as

$$S = \frac{\mu E}{V}$$

V = fluid velocity

Here one wishes to make S as small as possible.[8]

So, knowing the electric field and the fluid velocity, the slip can be calculated provided that the mobility is also know. Unfortunately, deducing the mobility is not straightforward since it depends on the size of the particle and on how it was charged[1]. If one plots the drift velocity defined in Equation 1 for the maximum field (breakdown) as a function of the radius for spherical water droplets in air at standard conditions, one gets the curves shown in Figure 1. Singly charged particles have a decreasing μE_b-velocity with radius because the drag is increasing while the electrical force remains constant. The case for particles charged to the Rayleight limit represents an upper bound in the charging scheme because more charges exceed the stability of the droplet at any given radius. Corona field charging is an intermediate case between the other two modes of charging. Since the speed of sound is

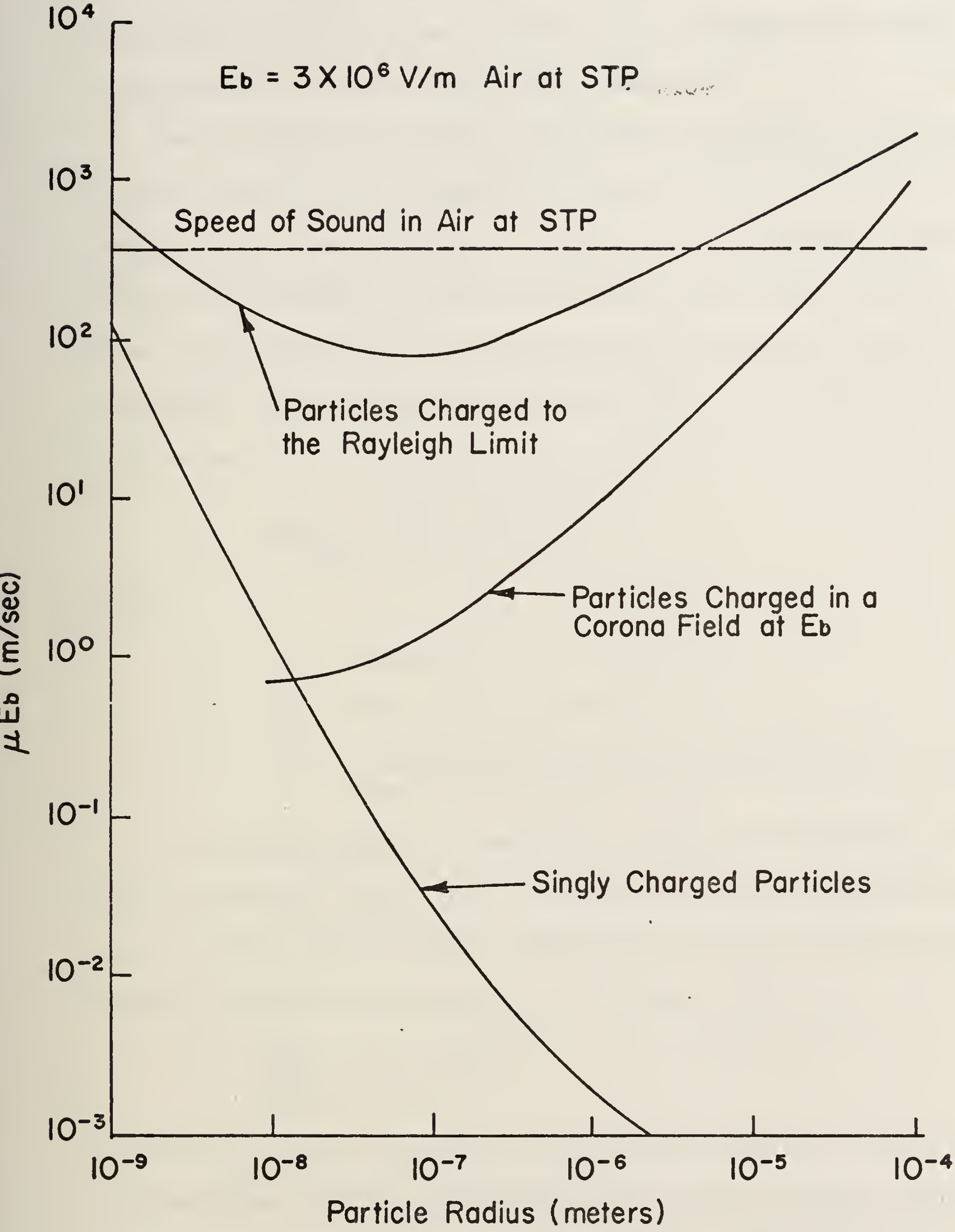

FIGURE 1. MAXIMUM DRIFT DUE TO ELECTRIC FIELD FOR WATER DROPLETS IN AIR AT 1-ATM AND 20°C

representative of flow velocities of practical interest, Figure 1 gives information about the range of radii and the charging scheme that would be required for a given value of the slip.

When the flow is unsteady, the question arises as to what happens to the conventional slip parameter. Clearly, inertial effects of the particles will come into play. In Appendix A, the momentum equation for a particle is treated. There a one-dimensional, spectral analysis is given which shows that the concept of the slip-parameter may be extended to unsteady flow. Written in a spectral form, the maximum value of the slip becomes

$$S(\omega)\big|_{max} = \frac{\mu E_b}{V(\omega)} + \omega\tau_v \tag{2}$$

where

ω = frequency

$V(\omega)$ = RMS spectral intensity

τ_v = e-folding time for the particle velocity to approach steady state value

τ_v (the equilibration time) is a function of the particle radius and of the viscosity of the fluid. If turbulence or any unsteady flow is to have an effect on the charges, then the slip parameter must be small for all the dominant frequencies (ω_k) of the flow, i.e.,

$$\frac{\mu E_b}{V(\omega_k)} + \omega_k \tau_v \ll 1.0$$

Actually, it is only necessary to look at the highest frequency of interest since for all smaller values of ω, the inequality above will be satisfied provided $V(\omega_k)$ retains nearly the same magnitude.

Figure 2 shows two curves bracketing a region in which the contribution of $\omega\tau_v$ to Equation 2 is between 10^{-3} and 10^{-2}. This range represents a criterion of small slip. The contribution of the first

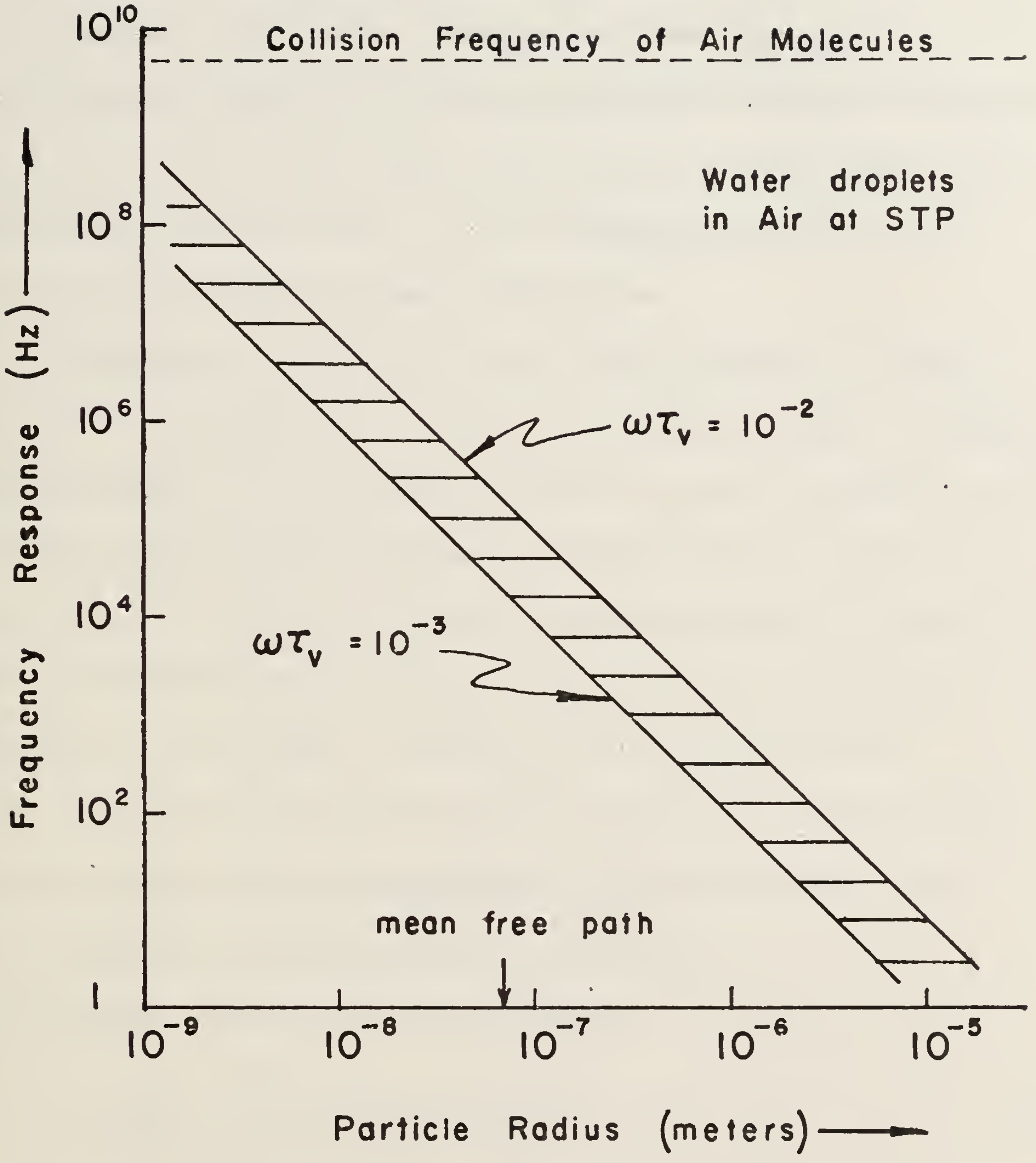

FIGURE 2. OPTIMUM FREQUENCY RESPONSE AS A FUNCTION OF THE RADIUS

term in the right-hand side of Equation 2 may or may not be as low as 10^{-2} but one would endeavor to pick a small enough value by manipulating with the charge of the particles (see Figure 1).

In Figures 1 and 2, water droplets have been described. For less dense particles or for hollow, spherical solids the curves move to the right (i.e., towards larger radii) which is a desirable effect from practical considerations. It is conceivable that one size of particle will be optimum for many applications.

The measurement of particle size, or more accurately stated of particle size distribution, is very difficult in the range of interest of EGD-anemometry[9,10]. The water droplets can only be measured in situ and direct techniques such as laser holography[11] can presently not measure below 50×10^{-6}m*. In the course of this work an indirect method of measurement was developed which consists of comparing the spectrum of the current collected to that of the hot-wire spectrum. For the proper particle size and charge distribution, the agreement between the two measurements is high when the flow has not been significantly disturbed by the particles.

The current collected may be written as

$$I_g(\omega) = \int_0^\infty v_p(\omega,R)q(R)\tilde{n}(R)dR \qquad (3)$$

where R = radius of the particle.

The total number of particles per unit volume, n_p, is

$$\int_0^\infty \tilde{n}(R)dR = n_p$$

and $q(R)$ = charge of the particle

$v_p(\omega,R)$ = velocity of the particle

Dividing Equation 3 by $v(\omega)$, the flow velocity, which is independent of the particle radius, one gets

$$\frac{I_g(\omega)}{v(\omega)} = \int_o^\infty \frac{v_p(\omega,R)}{v(\omega)} q(R)\tilde{n}(R)dR \qquad (4)$$

It is shown in Appendix B that the ratio $v_p(\omega,R)/v(\omega)$ may be approximated by a Heaviside-type of function,

$$\begin{aligned} \frac{v_p(\omega,R)}{v(\omega)} &= 1 \qquad & \tau_v \leq 1/\omega \\ &= 0 \qquad & \tau_v > 1/\omega \end{aligned}$$

This defines $R'(\omega)$, the radius at which τ_v equals ω^{-1} and Equation 4 becomes

$$\frac{I_g(\omega)}{v(\omega)} \approx \int_o^{R'(\omega)} q(R)\tilde{n}(R)dR$$

where for spherical particles

$$R'(\omega) = \left(\frac{9\mu_\infty}{2\omega\rho}\right)^{\frac{1}{2}}$$

μ_∞ = viscosity of fluid

ρ = particle density

Since one can obtain $I_g(\omega)$ and $v(\omega)$ experimentally, and since one can surmise what $q(R)$ must be, one can deduce the distribtuion $\tilde{n}(R)$ by solving the implicit equation above by successive approximations. $q(R)$ is given by the radius of the particle and the method of charging, as can be seen from Figure 1. If, however, the spread of particle size is narrow enough, then an average $\bar{q}$ per particle may be used as follows:

$$\frac{I_g(\omega)}{v(\omega)} = \bar{q} \int_o^{R'(\omega)} \tilde{n}(R)dR$$

or (5)

$$\frac{I_g(\omega)/\bar{q}n_p}{v(\omega)} = \frac{1}{n_p} \int_o^{R'(\omega)} \tilde{n}(R)dR$$

Therefore, the ratio of the "adjusted" value of the current to the fluid velocity represents the integral of the particle size distribution. When the radius $R'(\omega)$, equivalent to a particular frequency in question, is larger than that of the particles, the ratio of Equation 5 will be a constant. When it lies within the range of the particle size distribution, however, a decreasing value for this ratio will be seen as the frequency increases. At a high enough frequency, corresponding to radii smaller than the particles, the ratio will go to zero.

The hardware and the measurements are treated next before Equation 5 is further discussed.

IV. Experimental Set-Up

In the EGD apparatus, water droplets are introduced into an air-streams as depicted in Figure 3. The injector consists of an aerosol flow in conjunction with an ionizer. Saturated steam is injected through a corona discharge[12] into the turbulent wake of a cylinder. Electrons from the needle drift toward the attractor and attach themselves to the then-growing water droplets forming negative charged particles. This arrangement with the steam as the source of particles permits some variation of particle size distribution by mere manipulation of the steam pressure and temperature.

The anemometer is tested in a plexiglass wind-tunnel. The inside dimensions are five cm by ten cm in cross section and 25 cm in length. The test section contains the steam injector unit. The aerosol injector nozzle consists of a stainless steel ring 2.7 mm in diameter. This arrangement is shown in Figure 4.

The steel ring also serves as the corona ring positive electrode (attractor) of the aerosol ionizer. The negative electrode consists of a stainless steel needle. Typically at five millimeters downstream from

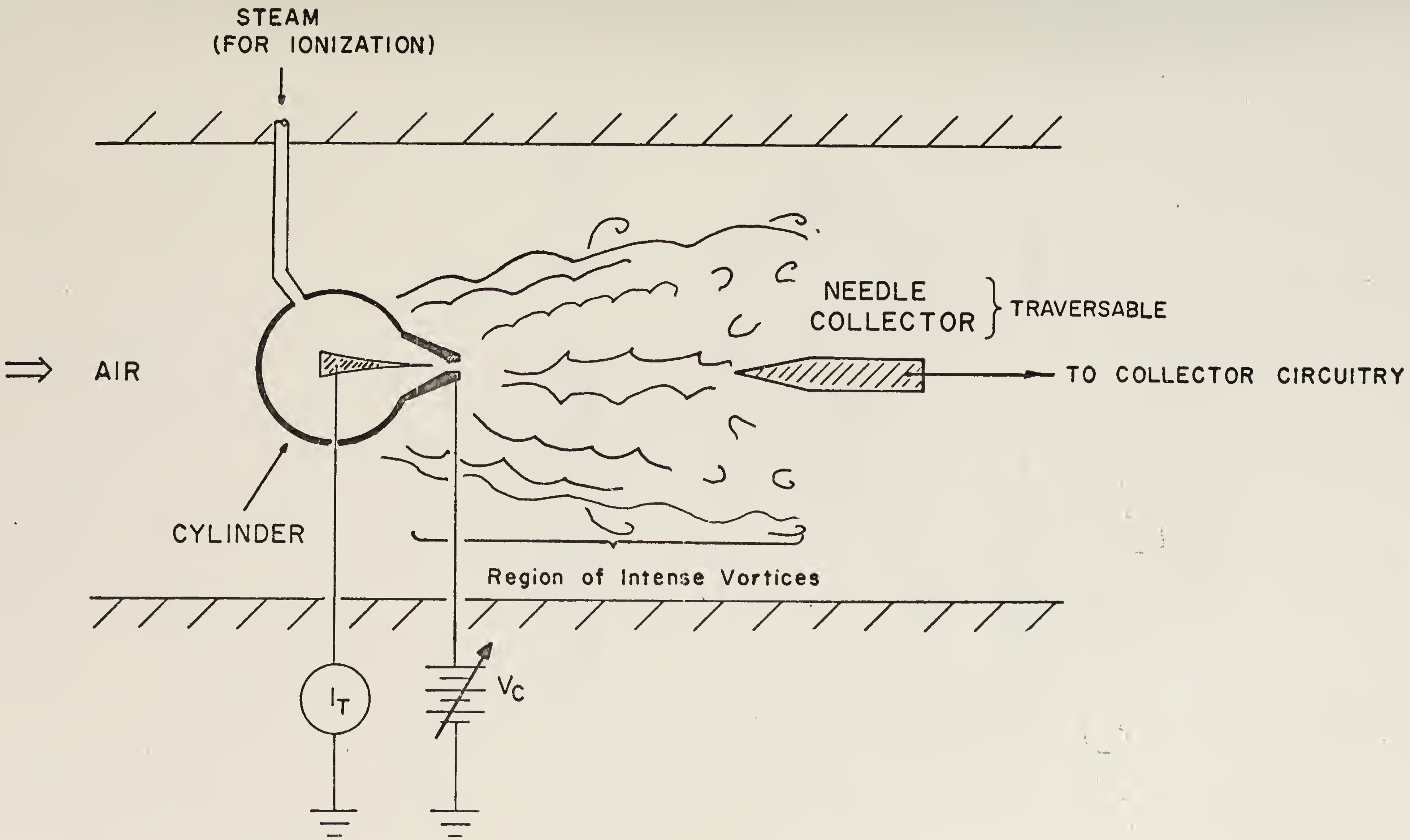

FIGURE 3. EGD GENERATOR SCHEMATIC

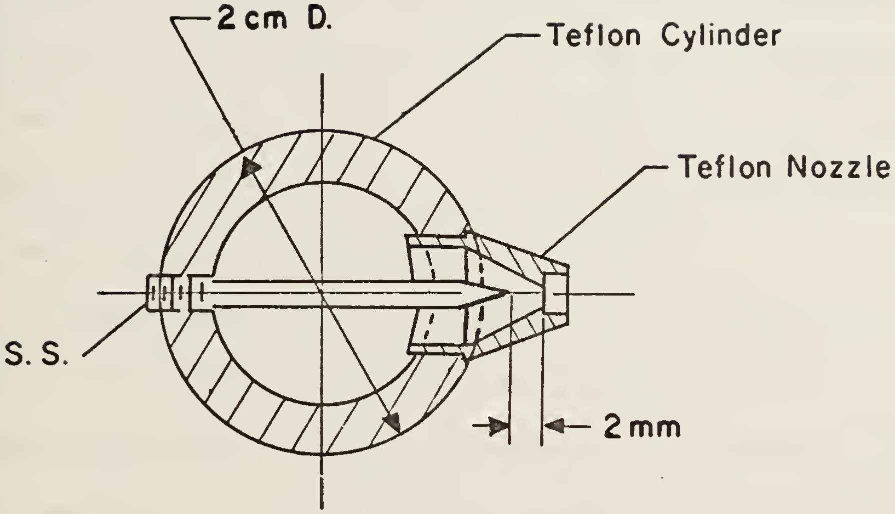

FIGURE 4. AEROSOL INJECTOR

the cylinder nozzle, a third electrode, in the form of a slender rod 1.5 mm diameter, collects the current. This separation distance is far enough downstream for equilibration between the particles and the flow to take place and close enough for substantial currents to be collected.

The air flow is fed through a temperature regulation stage for the control of the relative humidity since it was found that water droplets were somewhat affected by the humidity of the air during mixing outside of the nozzle. The humidity of the air was held at 32% because results were most reproducible at this value. (Humidity control would not be necessary with solid particles.) The water-air mixture flows out of the test section into the atmosphere.

The output from either the hot-wire or the EGD-collector probe is fed into a black box which houses the circuitry shown in Figure 5. The purpose of this black box is primarily for the protection of instrumentation downstream of the probe. The spectral data are obtained from a frequency analyzer. It is a General Radio Company Type 1920 Real Time Analyzer. It consists of a multifilter band-pass section and a multichannel RMS Detector. The signal from the preamplifier is fed into the multifilter, separated according to frequency, then fed into the RMS detector where the data are converted to binary digital form and the RMS level computed by true linear integration.

Hot-wire units of the constant-temperature type with frequency responses over 50 KHz were utilized. The hot-wire readings were used as a standard of comparison for the EGD measurements but, because the hot-wire calibration is not appropriate for two-phase flows, air was substituted for the steam in the cylinder. The air flow was matched so as to give the same momentum as the steam. The absence of droplets also helped prolong the life of the hot wires which was very marginal to begin

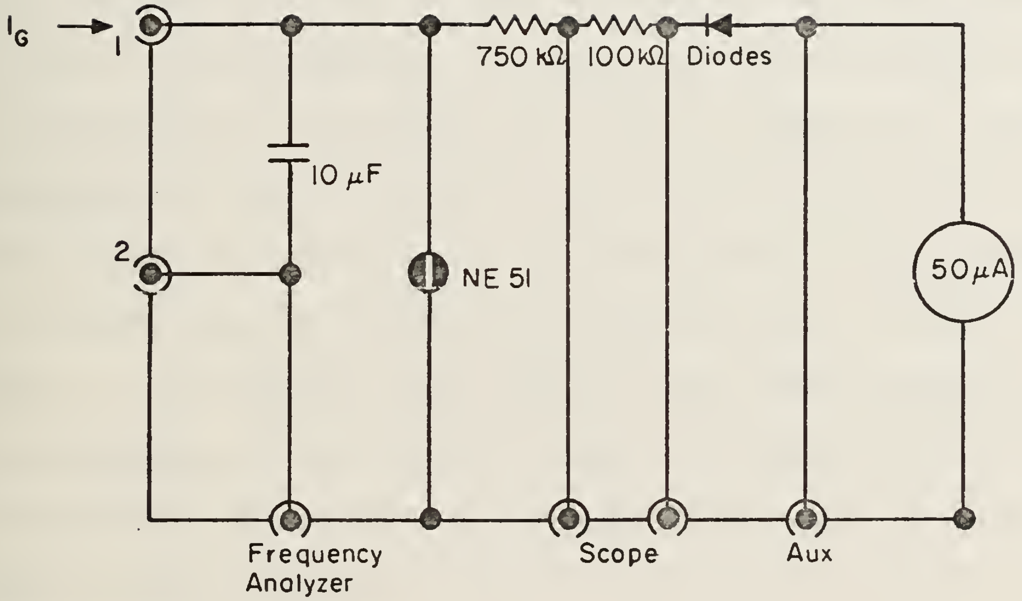

FIGURE 5.
ELECTRICAL SCHEMATIC OF COLLECTOR

with in the intense vorticity of the wake of the cylinder. The resulting hot-wire profile, after the temperatures of the two jets were equalized, is shown in Figure 6 for both the main air and nozzle air. There are two dominant frequencies apparent on this figure, namely, 1.2 KHz and 10KHz. The first one has the value of twice the Strouhal frequency for the cylinder and is appropriately so because measurements were taken along the centerline of the wake where the vortices shed-off by the cylinder on alternating sides add up. The Reynolds number based on the cylinder diameter for this flow (56 m/sec) is 8×110^4 so that the boundary layer on the cylinder is laminar before separation. The second important frequency in Figure 6 is associated with the nozzle for the steam--the inner jet. The 10 KHz peak appeared whether or not there was air issuing from this nozzle. The exit diameter for this nozzle is 2 mm which is some ten times smaller than the cylinder diameter and appropriately the frequency is nearly ten times higher. It was observed that 10 KHz is a high enough frequency so that the dissipation of the vortices is high; at a station 10 mm away from the nozzle exit the 10 KHz peak disappears whereas the 1.2 KHz peak remains nearly as intense.

V. Results and Discussion

The operation of the EGD-anemometer was investigated for frequency response and for current convection efficiency. The high frequency response was most noticeable when the steam was very close to the saturated condition before expansion (charges of 1°C noticeably affected the results). Because of this, it was decided to run the steam at two stagnation pressures to achieve different size of particles. Previous work in our laboratory[13] indicated that for the aerosol injector used and for an air flow of 56 m/sec, smaller droplets appeared at steam reservoir pressures below 1.6 atm.

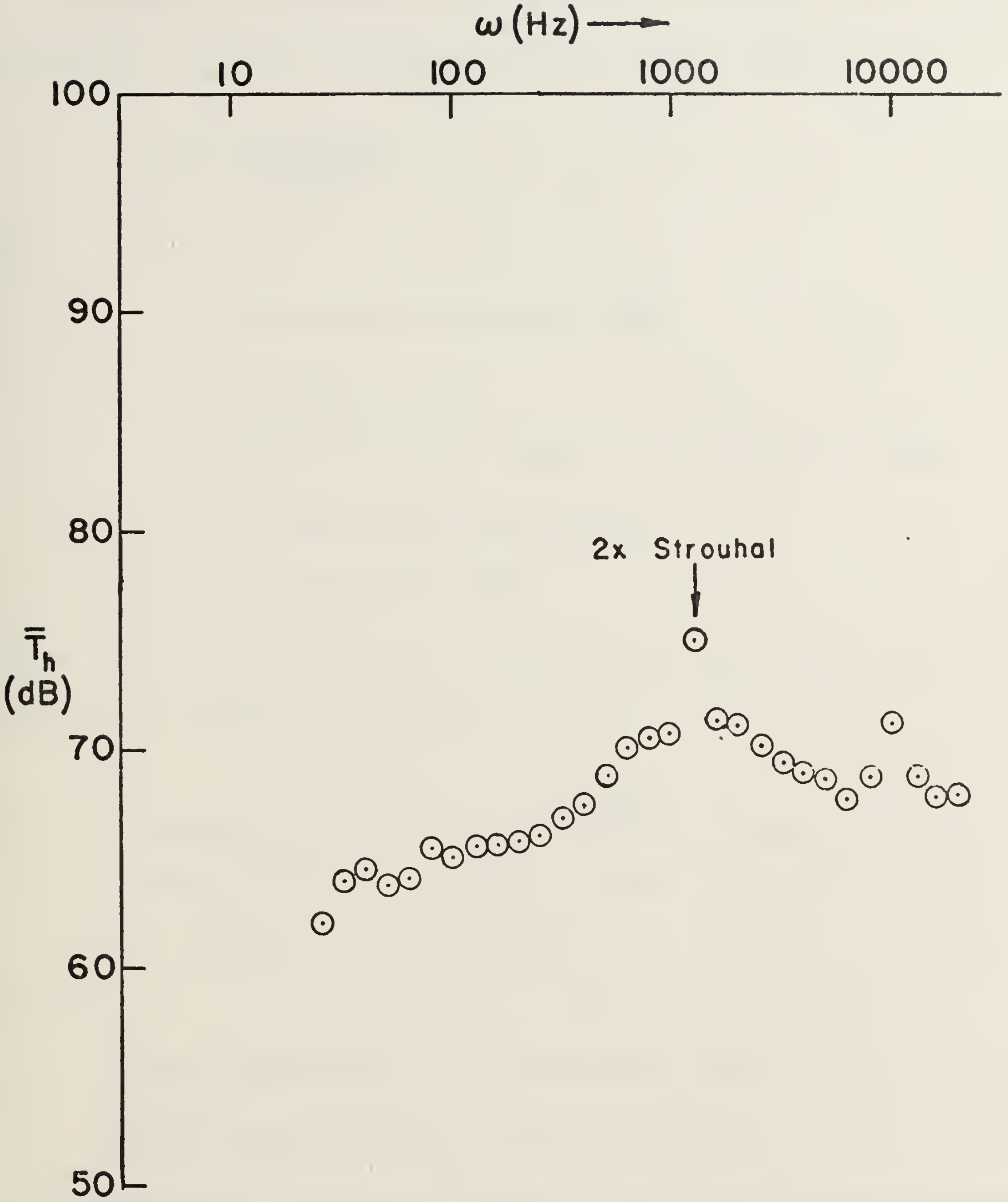

FIGURE 6. COMPOSITE OF HOT-WIRE ANEMOMETER DATA

The method of comparison between the EGD and hot-wire data is based on Equation 5. $T_g(\omega)$ is defined as an RMS parameter, namely,

$$T_g(\omega) \equiv \frac{I_{gn}/An_p\bar{q}}{v_n}$$

where

I_{gn} = spectral probe current (RMS)

A = collector area

n_p = total number of charge particles per unit volume

$\bar{q}$ = average charge per particle

v_n = flow velocity (RMS)

Letting u be a reference voltage (one millivolt in this case), one obtains for the value of T_g in dbs,

$$\underbrace{20 \log_{10}[T_g(\omega_n)]}_{\bar{T}_g(\omega_n)} = \underbrace{20 \log_{10} \frac{I_{gn}/An_p\bar{q}}{u}}_{\bar{T}_E(\omega_n)} - \underbrace{20 \log_{10} \frac{v_n}{u}}_{\bar{T}_h(\omega_n)} \qquad (6)$$

where

$\bar{T}_E(\omega_n)$ = measurement of the EDG-probe in dbs

$\bar{T}_h(\omega_n)$ = measurement of the hot-wire in dbs

The points shown in Figure 7 through 10, have the original EGD-probe data and a curve corresponding to the difference between those data and the hot-wire values of Figure 6. Twice the Strouhal frequency was chosen as a reference point in this comparison because it is the most intense point and because frequencies higher than 1.2 KHz are most sensitive to changes in the steam parameters.

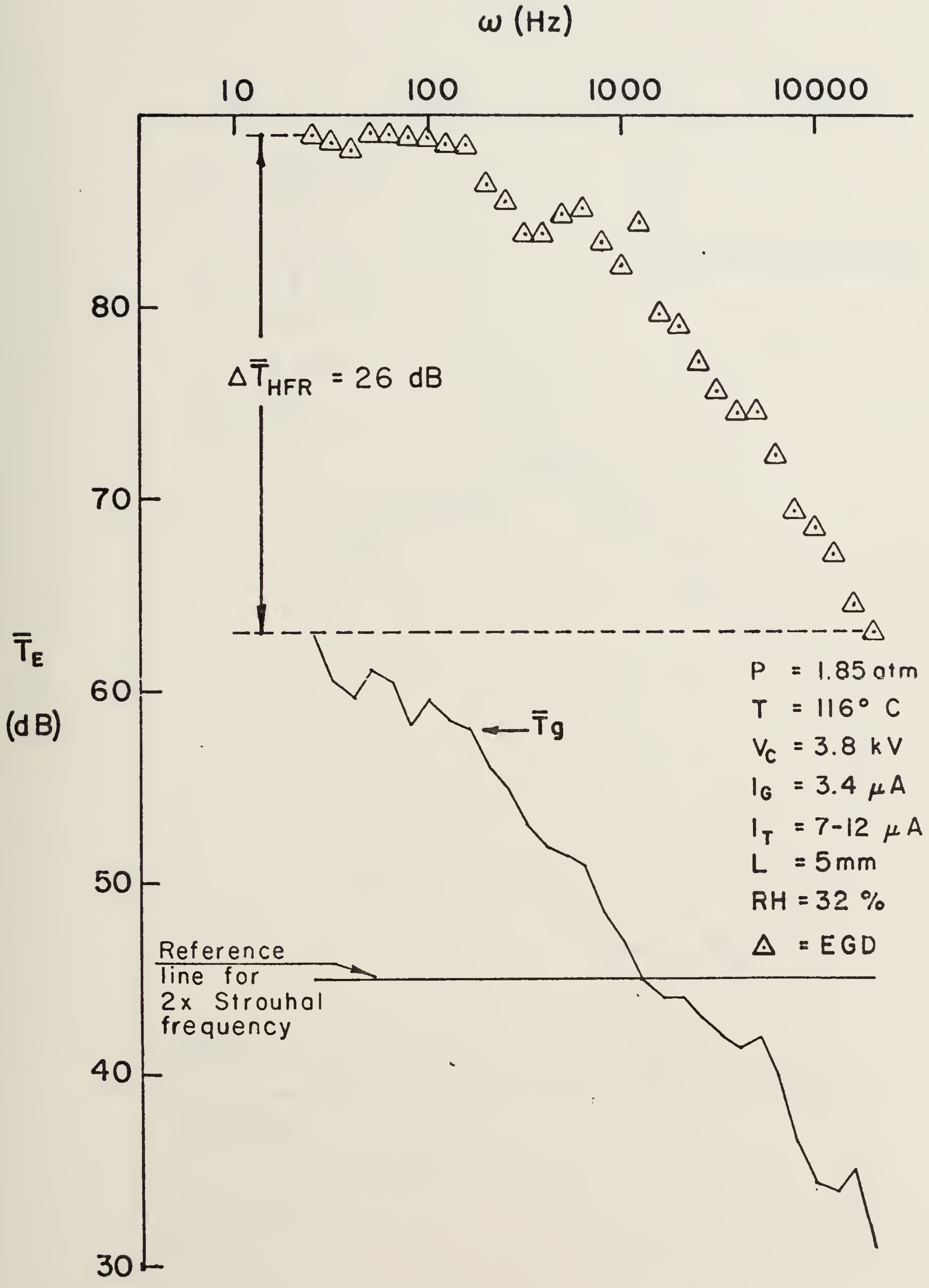

FIGURE 7. COMPARISON OF EGD AND HOT-WIRE DATA

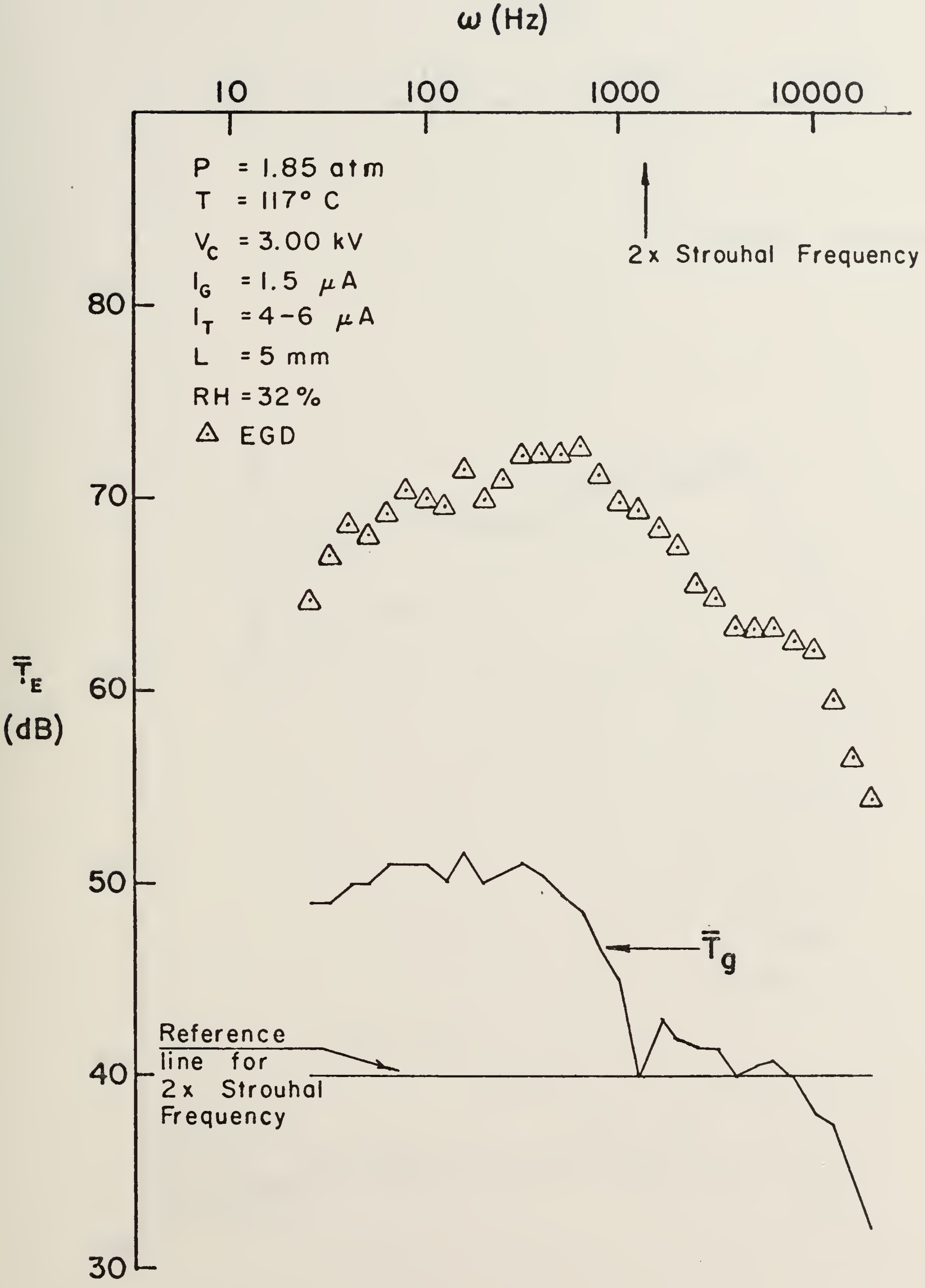

FIGURE 8. COMPARISON OF EGD AND HOT-WIRE DATA

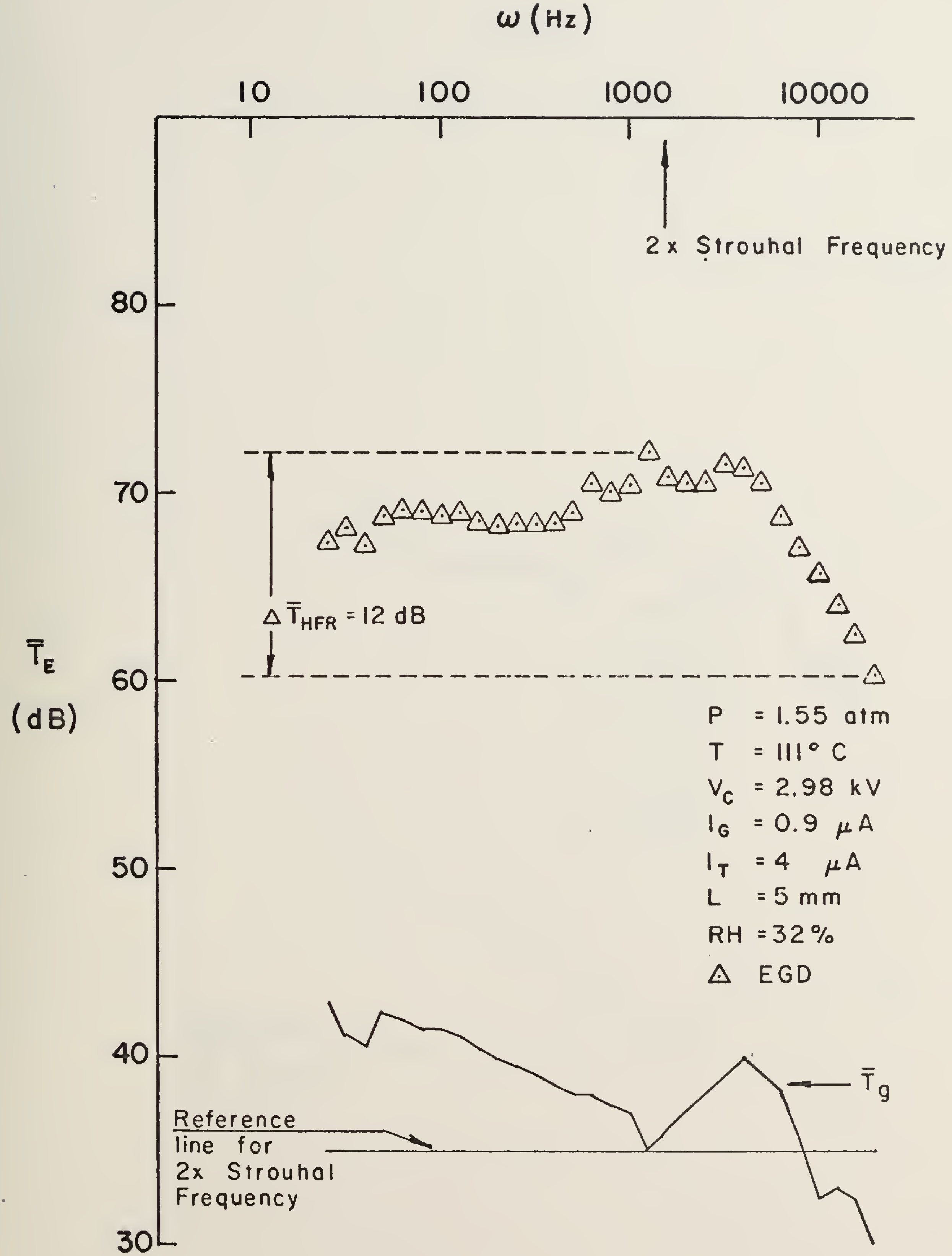

FIGURE 9. COMPARISON OF EGD AND HOT-WIRE DATA

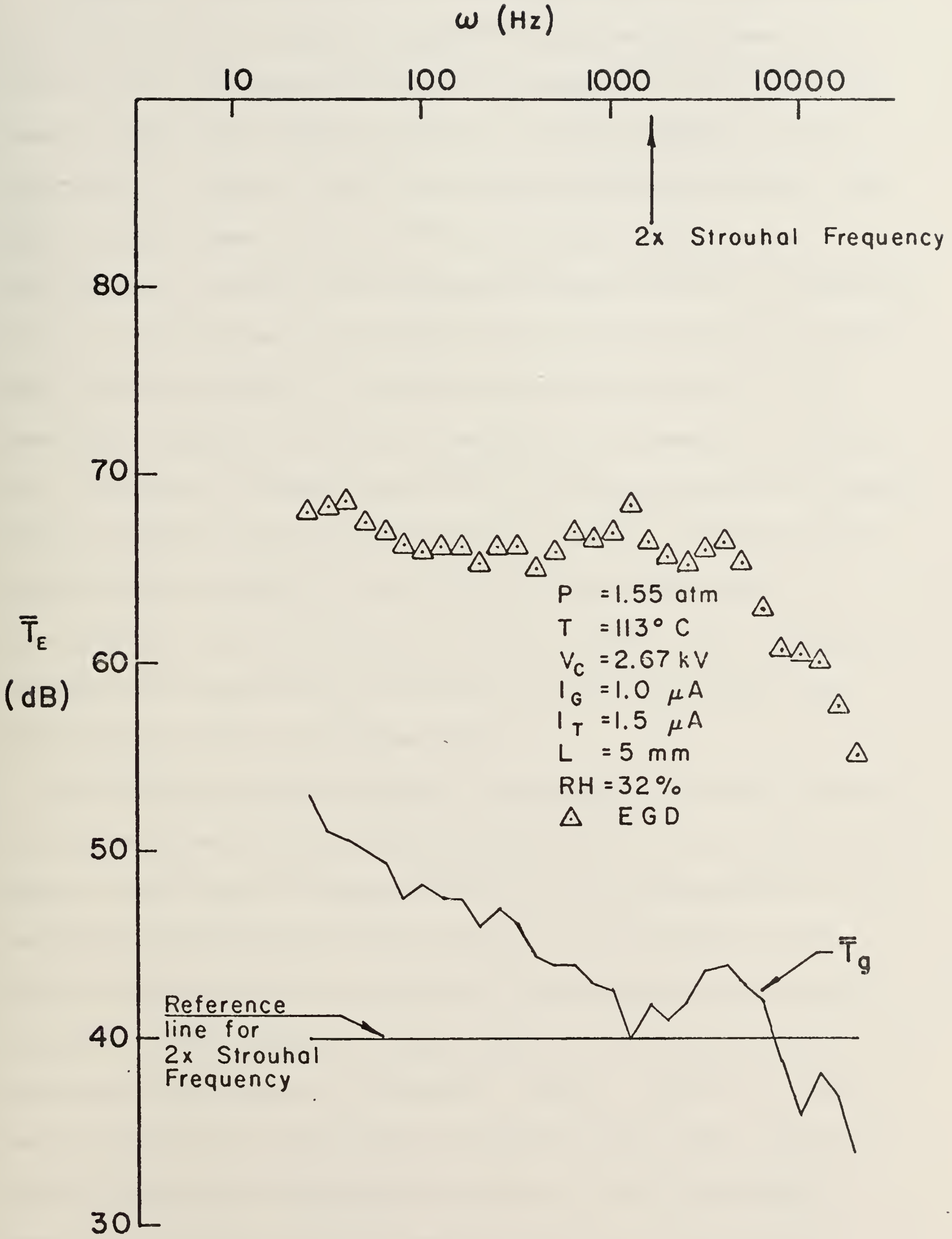

FIGURE 10. COMPARISON OF EGD AND HOT-WIRE DATA

Figures 7 and 8 show typical results for a steam reservoir pressure of 1.85 atm but with differing temperatures and corona voltages. At 1.85 atm, the corresponding saturation temperature is 118°C whereas the measured values were 116°C and 117°C for the data on Figures 7 and 8 respectively. Figures 9 and 10 show typical results at 1.55 atm. Here the saturation temperature is 113°C so it is clear that some supersaturation was achieved at both operating pressures before the expansion. If the curve for $\overline{T}_g$ were a horizontal line, then the two sets of measurements would only differ by a constant and the EGD anemometer would essentially reproduce the hot-wire anemometer measurements. An examination of Figures 7 through 10 shows that the present EGD-probe can measure intense turbulent fields with some degree of success. Figure 8 shows a correspondence of within ± 2dbs up to 630 Hz and Figure 9 shows a correspondence within ± 6dbs up to 20 KHz. The EGD - probe's response can be improved by operating with droplets of considerably smaller size distribution as will be discussed below.

The technique outlined earlier in this paper is entirely feasible for the measurement of particle size distribution. It is evident from Figures 7 and 8 that the data at 1.85 atm are well represented by the assumptions stated in Section III. There it was said that when the particle size distribution is such that it overlaps into the region of interest in the frequency scale (from Equation 5) then the amplitude of the signal will diminish in a monotonic fashion. The data in Figure 7 may be interpreted as indicating a distribution with center radius of 2×10^{-5} m and with a half-width of about 1.5×10^{-5} m (assuming a Gaussian distribution for the charged droplets and a corresponding average charge per droplet). The data in this figure have a correspondence with the hot-wire only up to about 80 Hz, which means that $R'(\omega)$ is

2.9×10^{-5} m. $R'(\omega)$ is essentially the higher value of the radius at the half-width. The data from Figure 8 has a correspondence with the hot-wire up to 630 Hz and this yields and $R'(\omega)$ of 1.2×10^{-5} m. The data at 1.55 atm, while having a better overall frequency response, do not show a monotonic decrease with increasing frequency. This implies the presence of more than one Gaussian distribution for the particles (the possibility of droplet fragmentation in the wake of the cylinder has been proposed[13]). It is evident that conditions outside of the nozzle strongly affect the droplet size and the statistical sample of data available at the present is too sparse to allow further conclusions. It can be seen from Figure 2, however, that a more favorable particle size distribution (i.e., centered about 10^{-7} m) would enhance the EGD-probe's response to match that of the hot-wire up to 20 KHz.

Turning now to other operating characteristics of the anemometer, Figure 11 shows the effect of the density of the steam on the current convection efficiency (I_g/I_T) for the two-phase fluid. In addition to the sensitivity of this efficiency to small changes in voltage, the effect of an increase in density is to require a higher voltage for the same efficiency. This shifting of the curves to the right is similar to that reported by Whitby[14] for the effect of pressure (temperature was held constant) in a single-phase fluid (air). Steam saturation effects are not apparent when pressure and temperature data are converted to density but they play an important role.

Figure 12 shows that a definite optimum voltage exists for operation with a good high frequency response. After a "triggering" voltage is attained the collector current increases linearly until finally a plateau is reached. The graph shows that the optimum current efficiency does not occur at optimum voltage although some preliminary observations indicated

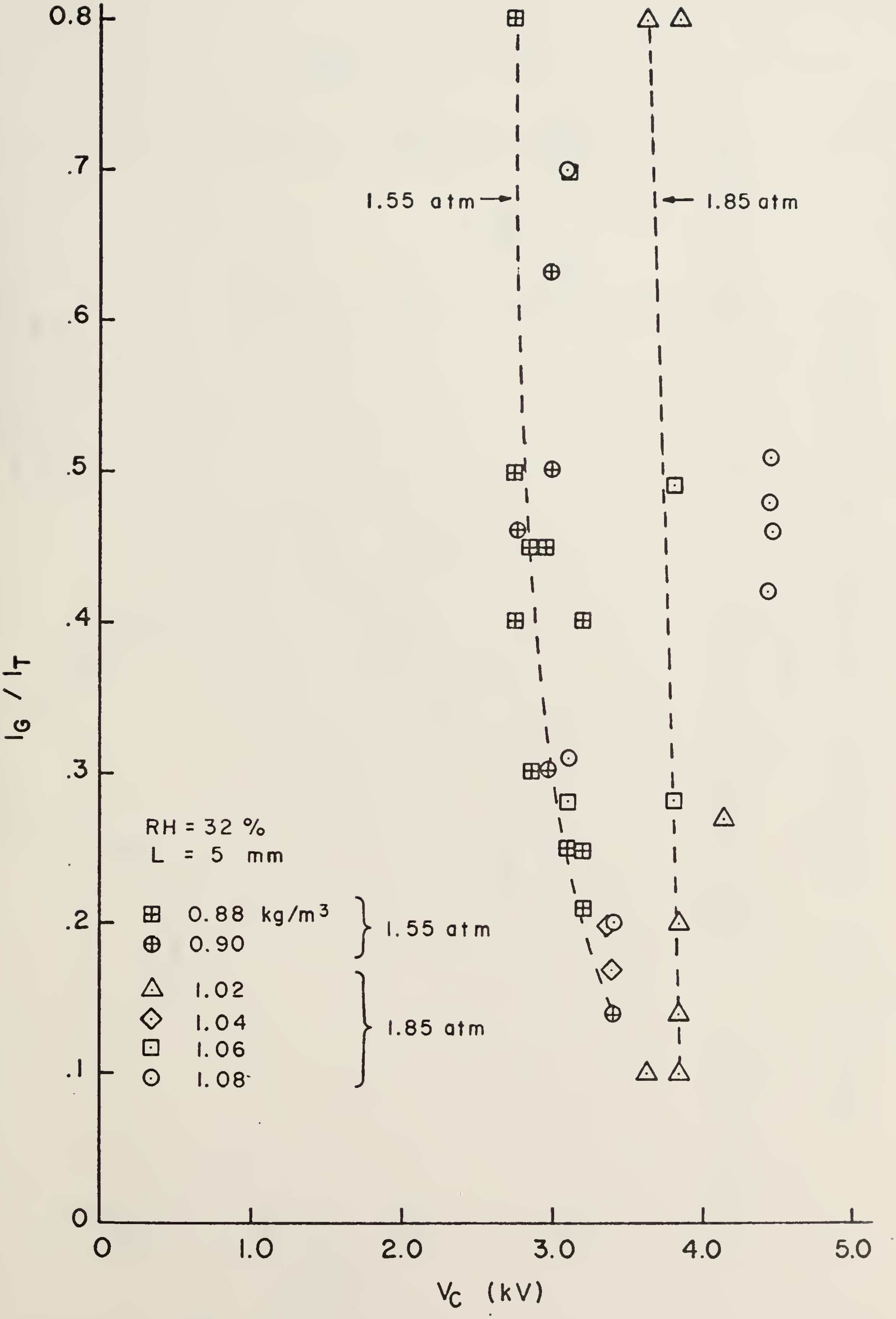

FIGURE 11. EFFECT OF DENSITY ON CURRENT EFFICIENCY

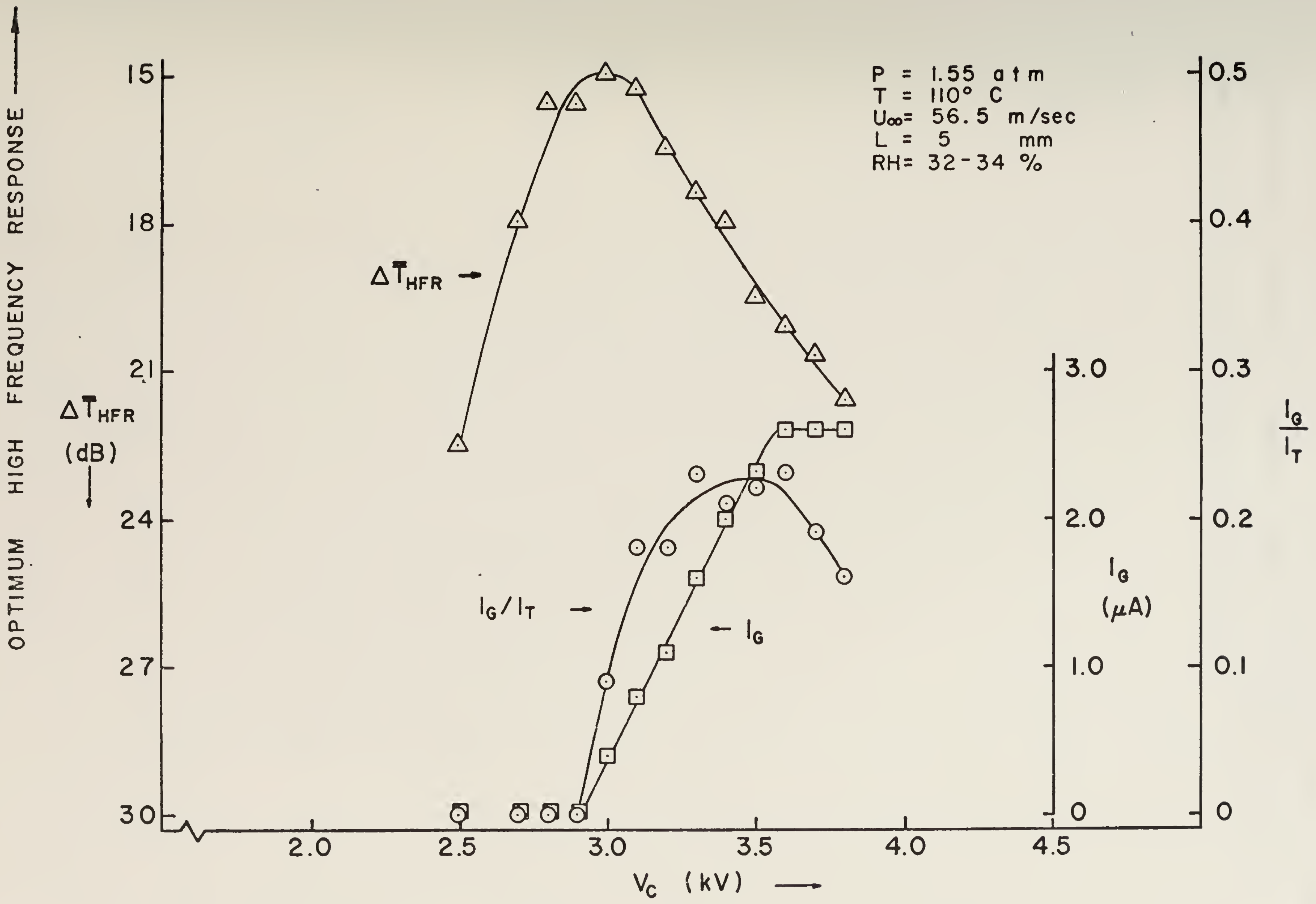

FIGURE 12. OPTIMUM VOLTAGE AND CURRENT

that acceptable results occurred at a current convection efficiency of 0.2 to 0.5 with higher collector currents. Figure 13 shows the effect of efficiency on the high frequency response for three different temperatures with other parameters held constant.

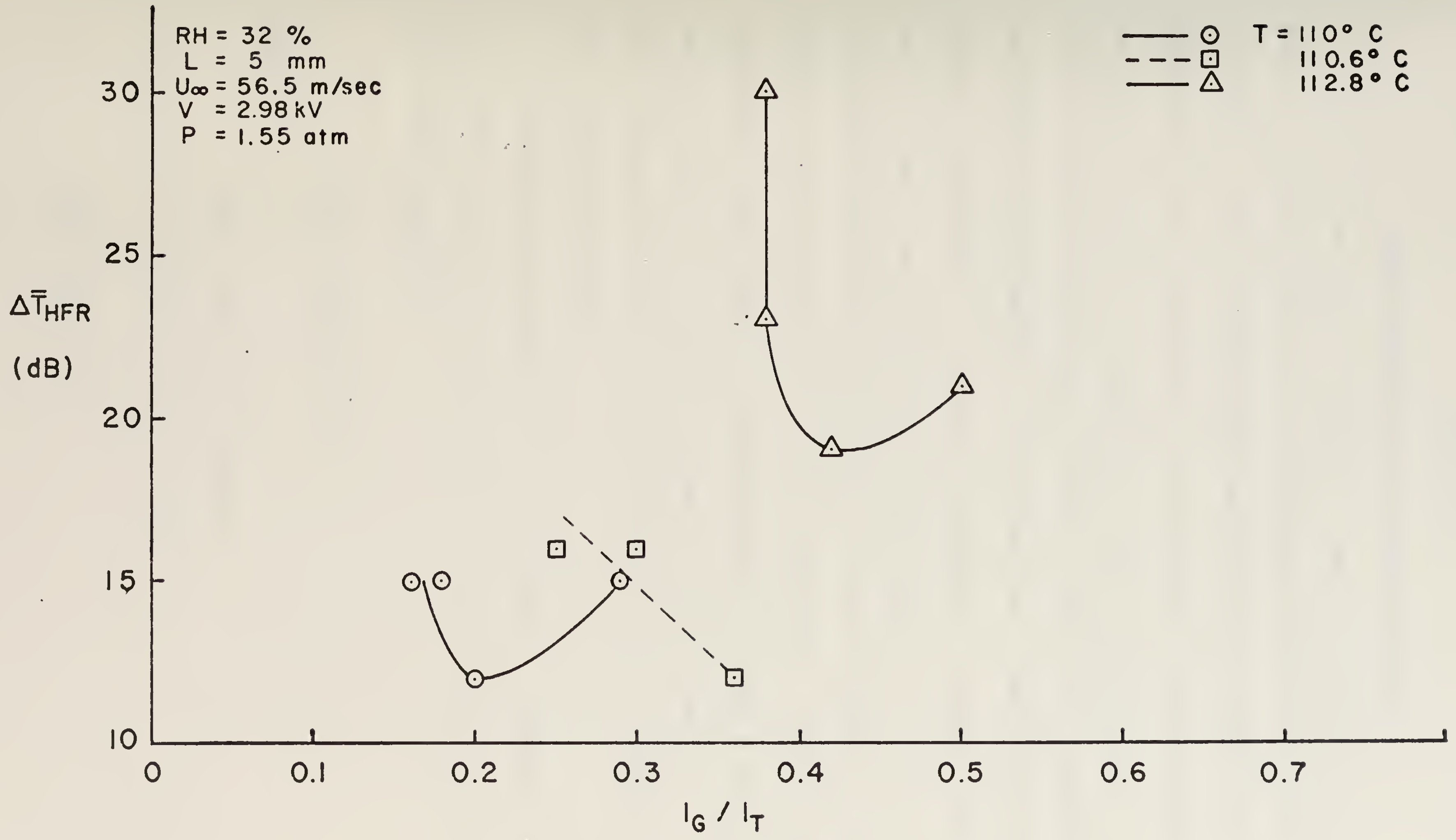

FIGURE 13.

EFFECT OF TEMPERATURE ON HIGH FREQUENCY RESPONSE AS A FUNCTION OF CURRENT EFFICIENCY

Appendix A

One-Dimensional, Spectral Analysis

For the case where the energy exchange between the flow and the electric field is slight, only the particle momentum equation is considered. The one-dimensional case depicted in Figure 14 is a useful simplification--it represents an extreme case where the entire fluid velocity is opposite to the electric field. In turbulent flows, this would be true only for part of the time. But one is interested here on an estimate of the maximum slip and hence on a description of the maximum interaction. The particle analyzed is assumed to be large enough to experience fluid dynamic drag forces (i.e., its diameter is greater than the mean free path of the gas molecules) but small enough so that pressure forces may be neglected. Stoke's drag is assumed applicable even though this overestimates the actual drag for Reynolds numbers (based on the particle diameter) which exceed one. In a restricted sense the particles size will be allowed to range to below the mean free path of the gas[15].

The free stream velocity "v" is divided in to spectral components at preselected frequencies ω_1, ω_2, ω_3, ... ω_n as follows: Let the velocity at a given location be

$$v(t) = \sum_n V(\omega_n) f(\omega_n, t)$$

where

$V(\omega_n)$ denotes the amplitude

and $f(\omega_n, t)$ is a periodic function with

$$|f(\omega_n, t)| = 1.0$$

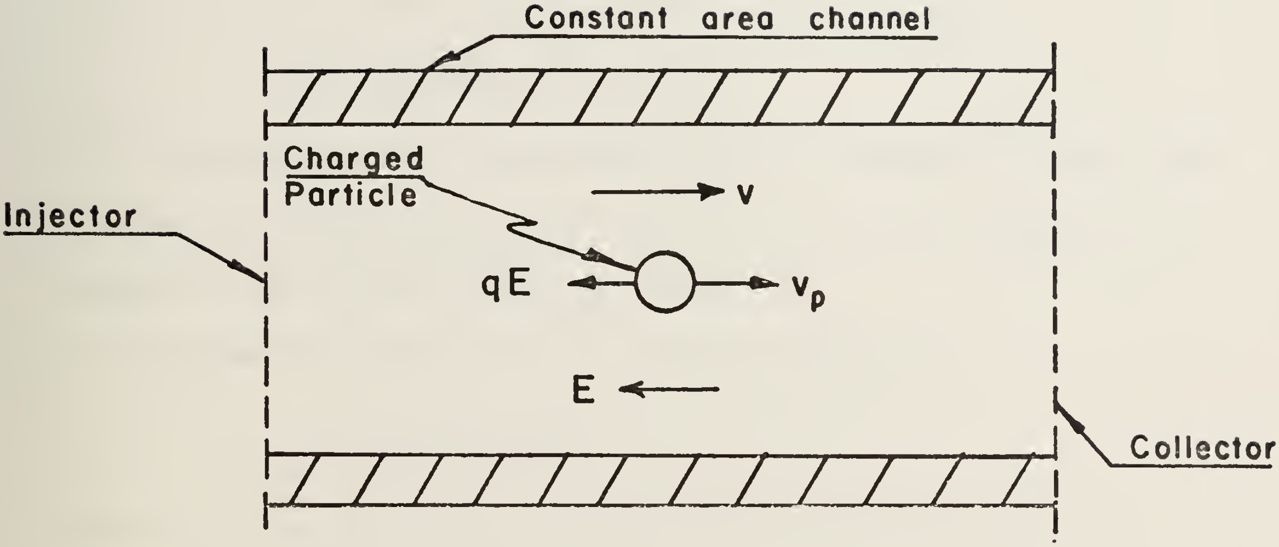

FIGURE 14. ONE-DIMENSIONAL MODEL

Now, at a given frequency ω_n, the particle momentum equation can be written as

$$m_p \frac{dv_p(\omega_n,t)}{dt} = \underbrace{6\pi R\mu_\infty[v(\omega_n,t) - v_p(\omega_n,t)]}_{\text{Stoke's Drag}} - \underbrace{qE}_{\text{Electric Force}} \tag{A1}$$

m_p = mass of the particle

R = radius of the particle (spherical shape)

μ_∞ = viscosity of the fluid

The electrical force is assumed steady here. There may be space charge fluctuations which influence "E" locally but these are assumed to be outside of the frequency range of interest.

The particle velocity can be similarly written as

$$v_p = \Sigma_n V_p(\omega_n)g(\omega_n,t)$$

where V_p is the amplitude and again $g(\omega_n,t)$ is periodic with $|g(\omega_n,t)| = 1.0$ so that Equation A1 becomes

$$m_p V_p(\omega_n) \frac{dg(\omega_n,t)}{dt} = \frac{m_p}{\tau_v}[V(\omega_n)f(\omega_n,t) - V_p(\omega_n)g(\omega_n,t)] - qE \tag{A2}$$

where

$$\tau_v \equiv \frac{m_p}{6\pi R\mu_\infty} \tag{A3}$$

which is the equilibration time for a constant velocity and no electric fields.

Now, if the particle mass (m_p) is vanishingly small, one gets the usual definition for the mobility from Equation A1, namely

$$v_D = v - v_p = \mu E \tag{A4}$$

where

$$v_D = \text{drift velocity}$$

$$\mu = \text{particle mobility} = \frac{q}{6\pi R\mu_\infty}$$

Before considering the inertia term as a perturbation, Equation A2 will be nondimensionalized. Let

$$\hat{t}_n = t\omega_n$$

so that for the ω_n particle, in simplified notation, one gets

$$m_p V_p \omega_n \frac{dg_n}{d\hat{t}_n} = \frac{m_p}{\tau_v}[v_n - v_{pn}] - qE$$

where

$$v_n = v(\omega_n, t) \text{ and } v_{pn} = v_p(\omega_n, t)$$

or

$$\underbrace{\left(\frac{m_p V_p \omega_n}{qE}\right)}_{O(\epsilon)} \underbrace{\frac{dg_n}{d\hat{t}_n}}_{O(1)} = \underbrace{\frac{m_p}{\tau_v qE}[v_n - v_{pn}]}_{O(1)} - 1 \qquad \text{(A6)}$$

From the above equation, one can see the perturbation parameter explicitly, namely,

$$\epsilon = \frac{m_p V_p \omega_n}{qE}$$

Now let

$$g_n = g_n^{(o)} + \epsilon g_n^{(1)} + O(\epsilon^2)$$

Substituting into Equation A6, collecting terms, and neglecting those of $O(\epsilon^2)$, one obtains

$$\frac{m_p}{\tau_v qE}[v_n - V_{pn} g_n^{(o)}] - 1 = 0 \qquad \text{(A7)}$$

and

$$\frac{d}{d\hat{t}_n}[g_n^{(o)}] = -\frac{m_p}{\tau_v qE}[V_{pn} g_n^{(1)}] \qquad \text{(A8)}$$

From the second of the two equations (Equation A8)

$$g_n^{(1)} = -\frac{\tau_v qE}{m_p V_{pn}} \frac{dg_n^{(o)}}{d\hat{t}_n}$$

Because E is assumed steady, Equation A7 replaces Equation A5, which defined the mobility. Moreover,

$$V_{pn} \frac{dg_n^{(o)}}{d\hat{t}_n} = -\frac{dv_n}{dt_n} = V_n \frac{df_n}{d\hat{t}_n}$$

so that Equation A8 becomes

$$g_n^{(1)} = -\frac{\tau_v qE}{m_p} \frac{V_n}{V_{pn}^2} \frac{df_n}{d\hat{t}_n}$$

and

$$v_{pn} = V_{pn} g_n = V_{pn}[g_n^{(o)} + \epsilon g_n^{(1)} + O(\epsilon^2)]$$

$$= v_n - \frac{\tau_v qE}{m_p} - \frac{V_n}{V_p} \frac{df_n}{d\hat{t}_n} \cdot \frac{m_p V_p \omega_n}{qE} \cdot \frac{\omega qE}{m_p}$$

or

$$v_{pn} = v_n - \mu E - \tau_v \omega_n V_n \frac{df_n}{d\hat{t}_n}$$

which is equivalent to

$$\boxed{v_{pn} = v_n - \mu E - \tau_v \frac{dv_n}{dt}}$$

The above equation is consistent with steady flow results and represents a first order perturbation of the particle velocity due to inertia effects.

Now, from Equation A4 the spectral drift velocity becomes

$$v_D(\omega_n,t) = V_n f_n - V_{pn} g_n = \mu E + \tau_v \omega_n V_n \frac{df_n}{d\hat{t}_n}$$

The spectral slip then becomes

$$S_n = \frac{\mu E}{V_n} + \tau_v \omega_v \frac{df_n}{d\hat{t}_n}$$

But by construction, it is reasonable to assume that

$$\left|\frac{df_n}{d\hat{t}_n}\right| = 1.0$$

hence

$$\boxed{S_n\Big|_{max} = \frac{\mu E_b}{V_n} + \tau_v \omega_n}$$

where $E = E_b$ is the breakdown field strength. Now V_n is the amplitude at the given frequency of the main flow and it is understood that where V_n is not significant (i.e., zero) the slip parameter has no meaning.

Now μ and τ_v are a function of the radius and μ in addition of the charge per particle which in turn is a function of the radius and the method of charging.

Appendix B

Effect of Particle Size Distribution

The current arriving at the probe is given by Equation 3, assuming one-dimensional flow.

$$I_g(\omega) = \int_o^\infty v_p(\omega,R)q(R)\tilde{n}(R)dR \tag{3}$$

where

$$\int_o^\infty \tilde{n}(R)dR = n_p$$

and v_p is the RMS value of the particle velocity.

In Appendix A, it was found that

$$v_{pn} = v_n - \mu E - \tau_v \frac{dv_n}{dt}$$

Since μE is independent of time, under the present assumptions the unsteady part of the above equation is

$$v'_{pn} = v'_n - \tau_v \frac{dv'_n}{dt} \tag{A9}$$

where the prime denotes the fluctuating components of the velocity. Therefore,

$$\frac{v'_{pn}}{v'_n} = 1 - \tau_v \frac{d}{dt} (\ell n\ v'_n) \tag{B1}$$

Now from a linearized version of the Navier-Stokes Equation[16],

$$v'_n = V_n \exp(-i\omega_n t)$$

where

$$i = \text{imaginary index}$$

Thus,

$$\frac{d}{dt}(\ell n\ v'_n) = -i\omega_n$$

and Equation B1 becomes

$$\frac{v_{pn}'}{v_n'} = 1 + i\omega_n\tau_v$$

Note that the above is time independent, so that its RMS value, taking the real part only, is

$$\frac{v_{pn}}{v_n} = (1 - \omega_n^2\tau_v^2)^{\frac{1}{2}} \qquad \text{(B2)}$$

Figure 15 shows a plot of this function for two arbitrary frequencies. It can be seen that because of the strong dependence of τ_v on the radius the function plots as a low-pass filter which may be idealized for the present purposes to a step function.

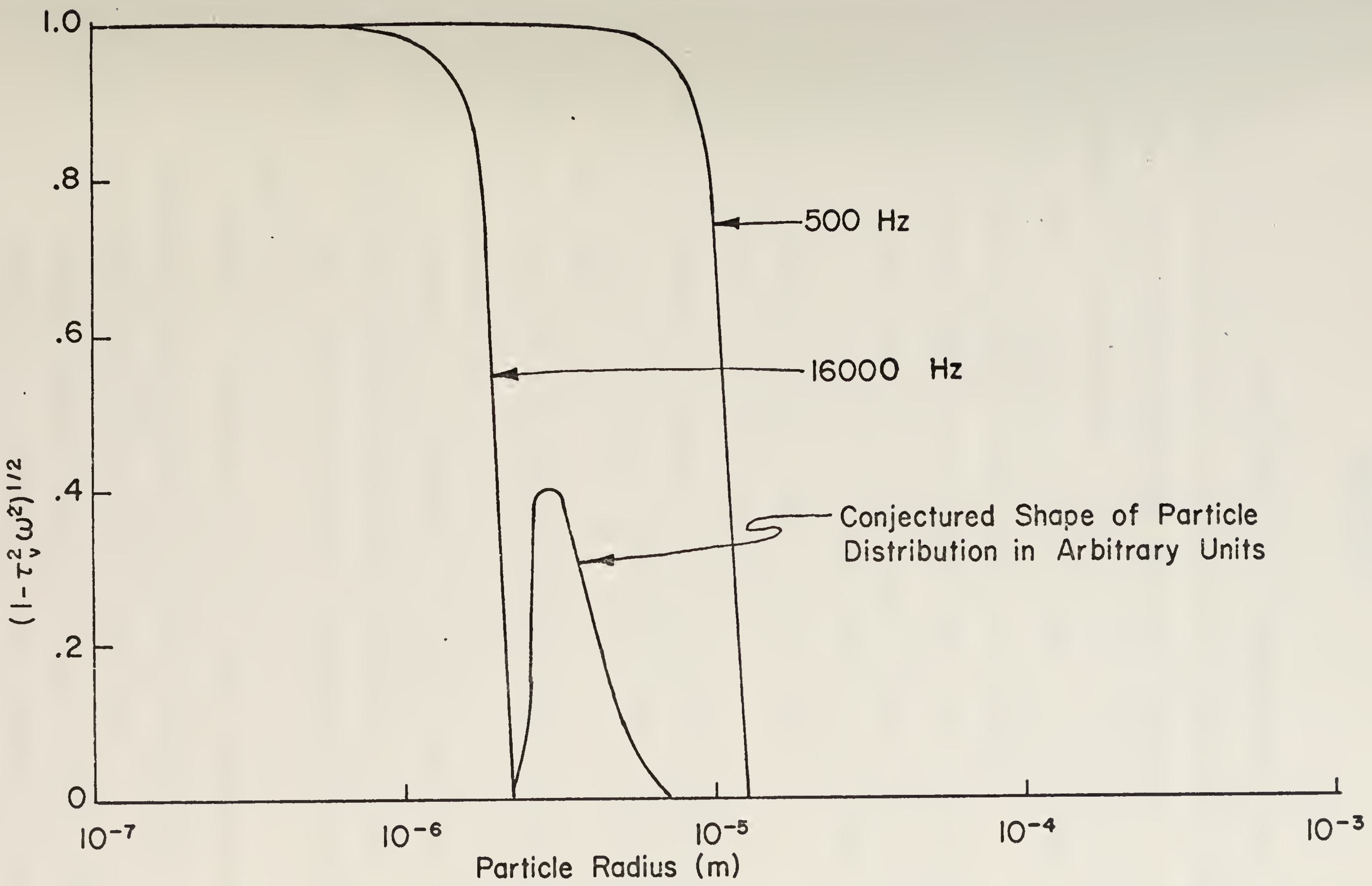

FIGURE 15. PLOT OF $(1-\tau_v^2\omega^2)^{1/2}$ VERSUS RADIUS FOR 500 HZ AND 16000 Hz

REFERENCES

*We attempted these measurements in our apparatus and 100μm was the best resolution available from our set up and no droplets were observed. The author would like to acknowledge the help of Professor D. J. Collins of the Naval Postgraduate School with the laser holographic measurements.

1) A. Marks, E. Barreto and C. K. Chu, AIAA J. 2, 45 (1964).

2) B. Karlowitz, Pure and Appl. Chem. 5, 557 (1962).

3) S. T. Demetriades, et al, Eleventh Symp. on MHD, Cal Tech, 64 (1970).

4) M. O. Lawson and F. Wattendorf (Eds) AGARDograph 122, 132 (1968).

5) J. O. Hinze, "Turbulence," (McGraw-Hill, New York, 1959) p. 122.

6) K. J. Nygaard, Rev. Sci. Instr. 36, 1771 (1965).

7) E. J. Durbin of Princeton University.

8) J. A. Decaire, M.O. Lawson, Eight Symp. on MHD, Stanford (1967).

9) G. B. Wallis, "One-Dimensional Two-Phase Flow," (McGraw-Hill, New York, 1969) p. 378.

10) H. C. Van de Hulst, "Light Scattering by Small Particles," (Wiley, New York, 1957).

11) B. J. Matthews, R. F. Wuerker, D. T. Harrje, Small Droplet Measuring Techniques, Technical Report AFRPL-TR-68-156, July 1958.

12) L. B. Loeb, "Electrical Coronas," (University of California Press, 1965).

13) O. Biblarz, K. E. Woehler, and T. H. Gawain, EHD Research, Naval Postgraduate School Report NPS-57Zi0121A, December 1970.

14) K. T. Whitby, Rev. Sci. Inst. 32, 1351 (1961).

15) J. D. Cobine, "Gaseous Conductors," (Dover, New York, 1958) p.33.

16) L. D. Landau and E. M. Lifshitz, "Fluid Mechanics," Pergamon, Oxford, 1959) p. 103.

DISTRIBUTION LIST

		No. Copies
1.	Defense Documentation Center Cameron Station Alexandria, Virginia 22314	2
2.	Library Naval Postgraduate School Monterey, CA 93940	2
3.	Commander Naval Air Systems Command Department of the Navy Attn: Dr. H. R. Rosenwasser, Code AIR-310C	1
4.	Chairman Department of Aeronautics Naval Postgraduate School Monterey, CA 93940	1
5.	Professor Oscar Biblarz Department of Aeronautics Naval Postgraduate School Monterey, CA 93940	5
6.	Mr. Alvin M. Marks Marks Polarized Corp. 153-16 10th Avenue Whitestone, NY 11357	1
7.	Professor A. E. Fuhs Department of Aeronautics Naval Postgraduate School Monterey, CA 93940	1
8.	Dr. Ralph Roberts Office of Naval Research Power Program, Code 473 Washington, DC 20360	1
9.	Mr. John A. Stakowski Office of Naval Research Power Program, Code 473 Washington, DC 20360	1

10. Dr. H. J. Mueller 1
Naval Air Systems Command
Code AIR 310
Washington, DC 20360

11. Dr. S. J. Magram 1
Army Research Office
Arlington, VA 22200

12. Air Force Office of Scientific Research 1
Washington, DC 20333
Attn: Power Systems Group

13. Mr. Robert C. Hamilton 1
Institute of Defense Analysis
400 Army - Navy Drive
Arlington, VA 22202

14. Dr. Geroge C. Szego 1
Institute of Defense Analysis
400 Army - Navy Drive
Arlington, VA 22202

15. Mr. S. Cohen 1
NASA Lewis Research Center
21000 Brookpark Road
Cleveland, OH 44135

16. Mr. M. Lawson 1
Aerospace Research Laboratory
U. S. Air Force
Wright-Patterson AFB, OH 45433

17. Dean of Research 1
Naval Postgraduate School
Monterey, CA 93940

U164244

DUDLEY KNOX LIBRARY - RESEARCH REPORTS
5 6853 01060355 8

~~U164244~~